Acta Crystallographica Section B
Structural Science
ISSN 0108-7681

Determination of the low-temperature structure of hexamethylbenzene

John A. Stride

Institut Laue–Langevin, 6 rus Jules Horowitz, F-38042 Grenoble, France

Correspondence e-mail: stride@ill.fr

Received 16 August 2004
Accepted 21 December 2004

The low-temperature structure of hexamethylbenzene has been determined from neutron powder diffraction data and found to differ from the room-temperature phase predominantly by a translation of molecular planes to a form a cubic close-packed type structure. By performing measurements as a function of temperature, the role of thermally induced agitation of the molecular units in the first-order phase transition is clearly demonstrated.

1. Introduction

Despite being somewhat ubiquitous in the chemistry laboratory, hexamethylbenzene (HMB) has remained enigmatic with respect to its low-temperature crystal structure. The presence of a low-temperature phase (referred to in the literature as phase III) was first discovered almost 75 years ago by calorimetry (Huffman *et al.*, 1930) shortly after the structure of the room-temperature phase (II) was first reported in 1929 (Lonsdale, 1929). This early structure refinement of Yardley–Lonsdale was one of the first full characterizations of a molecular material by single-crystal X-ray crystallography and the inherent confirmation of planar aromatic benzene units ended over 70 years of debate concerning the geometry of aromatic molecular systems. This work was further refined leading to a more comprehensive later study (Brockway & Robertson, 1939). The structure of II is triclinic under the $P\bar{1}$ space group, meaning that the asymmetric unit consists of one half of the molecule, with the molecule having a pseudo-threefold symmetry axis perpendicular to the molecular plane. The methyl groups lie slightly, 3.5 (3)°, out of the plane of the aromatic core, with alternate groups either above or below the C_6 plane (Le Maguères *et al.*, 2001).

Despite being recognized for over 70 years, the low-temperature phase III has proven to be stubbornly elusive and the literature is peppered with various attempts at solving this structural conundrum (Hamilton *et al.*, 1969; Fujiwara *et al.*, 1992). The situation is complicated by the tendency for single crystals of the material to shatter on passing through the phase transition at T_c^H = 117.5 (1) K, T_c^D = 132.4 (1) K (Fujiwara *et al.*, 1992). To date the lowest temperature complete refinement was performed on a fully protonated single-crystal sample at $T = 123$ K, $1.05T_c$ (Le Maguères *et al.*, 2001), and was found to be consistent with the published room-temperature data, with a cell volume contraction of 3%. Various techniques have been employed to investigate phase III; the apparent simplicity of the low-energy region of the vibrational spectra has led some workers to conclude on the presence of one molecule per unit cell (Ron & Hyams, 1972; Von Bougeard *et al.*, 1973), whilst other workers have favoured a cell occupancy

Table 1
Experimental details.

	T = 5 K	T = 140 K
Crystal data		
Chemical formula	$C_6(CD_3)_6$	$C_6(CD_3)_6$
M_r	180.39	180.39
Cell setting, space group	Triclinic, $P\bar{1}$ (No. 2)	Triclinic, $P\bar{1}$ (No. 2)
Unit-cell dimensions (Å, °)	a = 6.1803	a = 5.2360
	b = 6.190	b = 6.1845
	c = 6.1993	c = 7.9520
	α = 90.04	α = 103.82
	β = 90.13	β = 98.46
	γ = 90.24	γ = 100.06
V (Å^3)	237.15	241.36
Z	1	1
Calculated density (g cm^{-3})	1.263	1.241
Radiation type, wavelength (Å)	Neutron, 1.594	Neutron, 1.594
2θ range (°)	8.0–164.25	8.0–164.25
Data collection		
Diffractometer	Two-axis, powder	Two-axis, powder
Scan step width (°)	0.05	0.05
Refinement		
Refinement on	F^2	F^2
No. of observations	965	976
No. of parameters	10	9
R_{wp}	0.0895	0.0811

of 12 molecules from their X-ray Laue powder diffraction data (Celotti *et al.*, 1975). Fujiwara *et al.* (1992) reported the X-ray powder diffraction patterns of both h-HMB and d-HMB in phase III, but no mention was made of attempts to index the patterns or to solve the structure. Amongst the non-structural methods used to investigate III, recent Raman measurements as a function of both temperature and applied pressure indicate that the first-order phase transition from II to III has a significant contribution from the intramolecular torsion of the methyl groups (Me; Takeshita *et al.*, 1999), consistent with the large isotopic shift in the transition temperature (Fujiwara *et al.*, 1992). Also, we have very recently reported (Adams *et al.*, 2004) on inelastic neutron scattering measurements which both advance earlier neutron diffraction work (Hamilton *et al.*, 1969) and support the notion of single-molecule unit-cell occupancy. Meanwhile, solid-state NMR has shown that neighbouring Me groups in HMB are strongly coupled and that below T_c the Me torsions are also coupled to whole molecule reorientations (Takeda & Chihara, 1987; Takeda *et al.*, 1980). Thus, the experimentally determined tendency toward the strong Me coupling limit, often referred to as Me-gearing, is in accordance with the computational studies of HMB, which have consistently hinted at such an effect (Iroff, 1980; Gough *et al.*, 1985).

The motivation for this work is then clear to see; the long-standing conundrum of the structure of the low-temperature phase in HMB is ripe for further study. Neutron powder diffraction has been used to obtain the structure of d-HMB at a series of temperatures about the II/III transition and the current study constitutes the first full determination of the structure in phase III. In addition, a low-temperature measurement of h-HMB using synchrotron radiation was found to largely confirm these findings.

2. Experimental

Neutron measurements were performed on the D2b two-circle neutron diffractometer at the ILL, France, using neutrons of incident wavelength λ = 1.594 Å (Hewat, 1986). The sample [2.5 g of $C_6(CD_3)_6$, 99% purity] was placed into a hollow vanadium cylinder of 40 mm height and inserted into a cryostat to obtain the low sample temperatures. Measurements were performed over $8.0 \leq 2\theta \leq 164.25°$ with a step size of 0.05° and at seven temperatures, T = 5, 80, 110, 125, 129, 132 and 140 K. The aluminium tail of the cryostat led to an anomalous peak in the diffraction pattern at around $2\theta \simeq 151°$, leading to an excluded region which spreads over 3.5° between 150.5 and 154° in the measured data.

Synchrotron data were obtained on the beamline ID31 (previously BM16) at the ESRF, France, at an incident wavelength of λ = 0.80 Å (Fitch, 2004). The ∼ 10 mg sample of $C_6(CH_3)_6$, 99.9% purity, was loaded into a thin-walled glass capillary and mounted onto a rotating sample stick in an attempt to reduce the problem of preferred orientation in the small X-ray beam. An He flow cryostat was used to obtain a sample temperature of T = 20 K. Data were recorded over the angular range $4.002 \leq 2\theta \leq 53.055°$ with a step size of 0.0005° (later re-binned to 0.003°). Under the experimental condi-

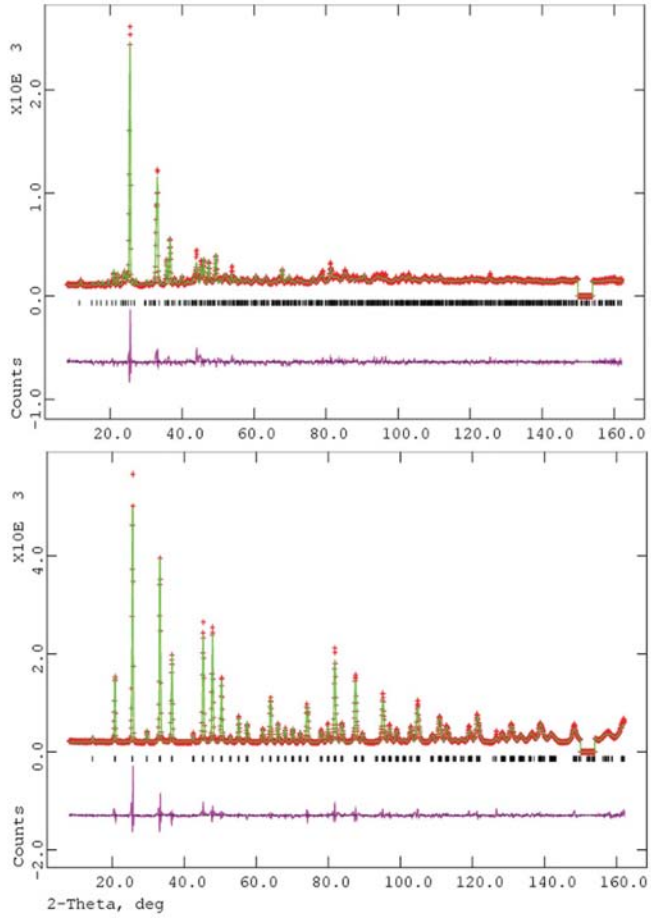

Figure 1
Final Rietveld plots at T = 140 K (upper) and T = 5 K (lower).

tions, the intrinsic instrument resolution is broadened by the sample microstructure to *ca* 0.02°.

All samples were obtained from the Aldrich Chemical Co. and used without further purification.

3. Results and discussion

The refinement of the low-temperature neutron diffraction data was performed in two stages. Using the recent single-crystal structure of h-HMB in II of Le Maguères *et al.* (2001) at T = 123 K as a starting geometry, a simulated annealing routine using *Cerius*2 (Molecular Simulations Inc., 1995) was applied to obtain an estimate of the structure in III. This process has been described elsewhere for similar systems (Neumann *et al.*, 2001) and so only a brief outline of the method is given here. Initially, the starting geometry was corrected for perceived errors in the C—H distances before being allowed to relax *via* rigid bodies, consisting of the benzene ring, and each of the six Me groups, totalling 9 degrees of freedom (X,Y,Z-rotation of the ring and 6 methyl torsions) without symmetry constraints. The simulated annealing procedure produced a structure which was consistent with $P\bar{1}$ symmetry, *i.e.* having an inversion centre at the $(\frac{1}{2},\frac{1}{2},\frac{1}{2})$ position. This was then fully refined by a Rietveld analysis (Rietveld, 1969) using the *GSAS* program (Larson & Van Dreele, 2000) to obtain the cell parameters, fractional atomic coordinates and isotropic atomic displacement parameters for each of the atoms in the cell at T = 5 K. The quality of the fit was assessed using the weighted residual R_{wp} and was reduced to 0.0895, which compares reasonably well to that obtained for the single-crystal determination of Le Maguères *et al.* (2001), R_1 = 0.0469, wR_2 = 0.1330. This structure was then used as the starting structure in the Rietveld refinement of the T = 80 K data, which was then used in the subsequent temperature refinement. Hence, a cyclical refinement method was used to obtain model structures up to T_c. The structure at T = 140 K was obtained directly from the initial starting geometry of Le Maguères *et al.* (2001), with a final $R_{\rm wp}$ = 0.0811, similar to that obtained at T = 5 K in phase III, Table 1. The final structural atomic parameters have been deposited[1] and an example of the fits for T = 5 K and T = 140 K are shown in Fig. 1.

As can be seen in Table 1, the unit cell in phase III is very close to being cubic with $a \simeq b \simeq c$ and $\alpha \simeq \beta \simeq \gamma \simeq 90°$, resulting in a large degree of coincidence in the observed Bragg peaks, meaning that the observables are much reduced as each *hkl* reflection is overlapped by all of the possible permutations of *hkl*, including the interchange of sign. This overlap, of up to 48 reflections in the general case, did not permit a full refinement of the peak profile parameters and so only the three principal terms and the asymmetry of the multi-term Simpson's rule integration method, based upon the pseudo-Voigt line-shape (Howard, 1982), were refined. An attempt to overcome the problem of heavily overlapped peaks led to synchrotron X-ray experiments at a much higher angular resolution. The synchrotron data was indexed using a Pawley refinement (Pawley, 1981) within the Materials Studio software package (Accelrys Inc., 2003), $R_{\rm wp}$ = 0.0084. All powder lines in the synchrotron data were found to be broadened beyond the intrinsic instrument resolution, ruling out the possibility of observing fine structure within the peak profiles. A Rietveld refinement of the data, based upon the low-temperature neutron structure, terminated at R_p = 0.0718, $R_{\rm wp}$ = 0.1316, with a = 6.2102, b = 6.2047, c = 6.2200 Å, α = 90.15, β = 90.01, γ = 90.26° and V = 239.67 Å^3. It is of interest to note here that the low-temperature h-HMB cell data is ∼ 1% larger in volume than the d-HMB data, as is the case for the T = 123 K ($1.05T_C^H$) h-HMB data of Le Maguères *et al.* (2001) and the corresponding T = 140 K ($1.05T_C^D$) d-HMB data. This discrepancy in cell volumes is consistent with the increased zero-point motion of hydrogen with respect to

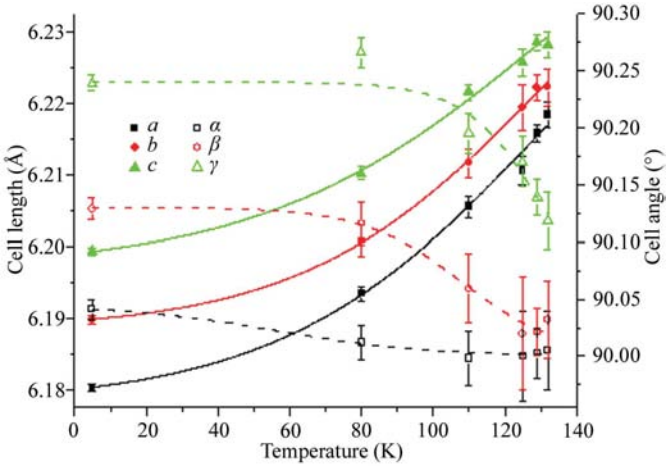

Figure 2
Systematic variation of unit-cell parameters of HMB in the low-temperature phase III determined by indexing of the diffraction patterns.

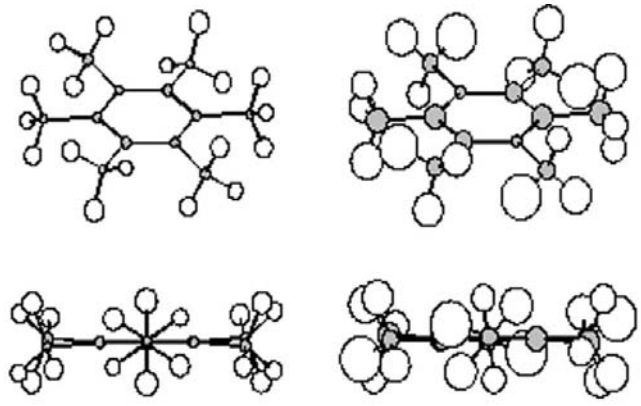

Figure 3
Molecular geometry of HMB in phase III (left) and phase II (right) detailing the isotropic displacement parameters obtained in the Rietveld refinement of the data. The concerted staggering of methyl groups is clearly shown in the views along the molecular plane.

[1] Supplementary data for this paper are available from the IUCr electronic archives (Reference: LC5016). Services for accessing these data are described at the back of the journal.

Table 2
Refined unit-cell parameters of HMB as a function of temperature.

Temperature (K)	a (Å)	b (Å)	c (Å)	α (°)	β (°)	γ (°)	V (Å^3)
5	6.1803 (5)	6.1898 (6)	6.1993 (5)	90.041 (9)	90.129 (9)	90.239 (7)	237.15 (4)
80	6.193 (1)	6.201 (1)	6.210 (1)	90.01 (2)	90.12 (2)	90.27 (1)	238.49 (7)
110	6.206 (2)	6.212 (2)	6.221 (1)	90.00 (2)	90.06 (3)	90.20 (2)	239.81 (11)
125	6.211 (2)	6.219 (3)	6.226 (2)	90.00 (4)	90.02 (5)	90.17 (2)	240.47 (16)
129	6.218 (2)	6.222 (2)	6.228 (1)	90.00 (2)	90.02 (2)	90.14 (2)	240.88 (9)
132	6.218 (2)	6.222 (3)	6.228 (2)	90.01 (4)	90.03 (3)	90.12 (3)	240.98 (14)
140	5.2360 (8)	6.1845 (8)	7.952 (1)	103.82 (1)	98.46 (1)	100.06 (1)	241.36 (6)

deuterium (Mizuno *et al.*, 2004). The limitation in the synchrotron data is believed to be due to preferred orientations within the small sample volume illuminated in the synchrotron experiment and despite the use of a rotating sample cell and a March–Dollase preferred orientation algorithm in the Rietved refinement (Dollase, 1986), a satisfactory solution was not found. However, the treatment of the synchrotron data acts to largely confirm the neutron data and in particular the closeness of the unit cell of phase III to a cubic form. The use of very much larger sample volumes in neutron powder diffraction experiments ensures adequate averaging over individual crystallite orientations, resulting in a better powder pattern. A similar example of this same problem was recently reported in the low-temperature structure determination of methane (Neumann *et al.*, 2003). Further evidence in support of the structure determinations in phase III is the systematic variation of all the cell parameters as a function of temperature, Fig. 2 and Table 2. As T_c is approached from below, the cell apparently moves towards a more cubic form, with $a \simeq 6.23$ Å ($V \simeq 241.8$ Å^3), but collapses into the room-temperature phase II before reaching the cubic geometry.

Indeed, the *closeness* of the cell to that of the cubic form for phase III construes a pseudo-rhombohedral space-group symmetry on the system. However, attempts to refine the structure to the higher-symmetry $R3m$ space group, with the C atoms lying on special positions (3*a* sites), were unsuccessful. The structure of phase III has the normal to the plane of the benzene rings approximately along the (111) direction with

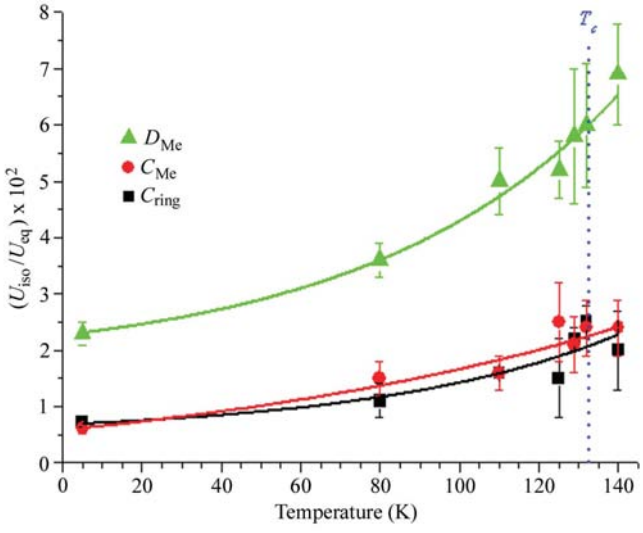

Figure 4
Average isotropic atomic displacement factors in HMB as a function of temperature for phase III.

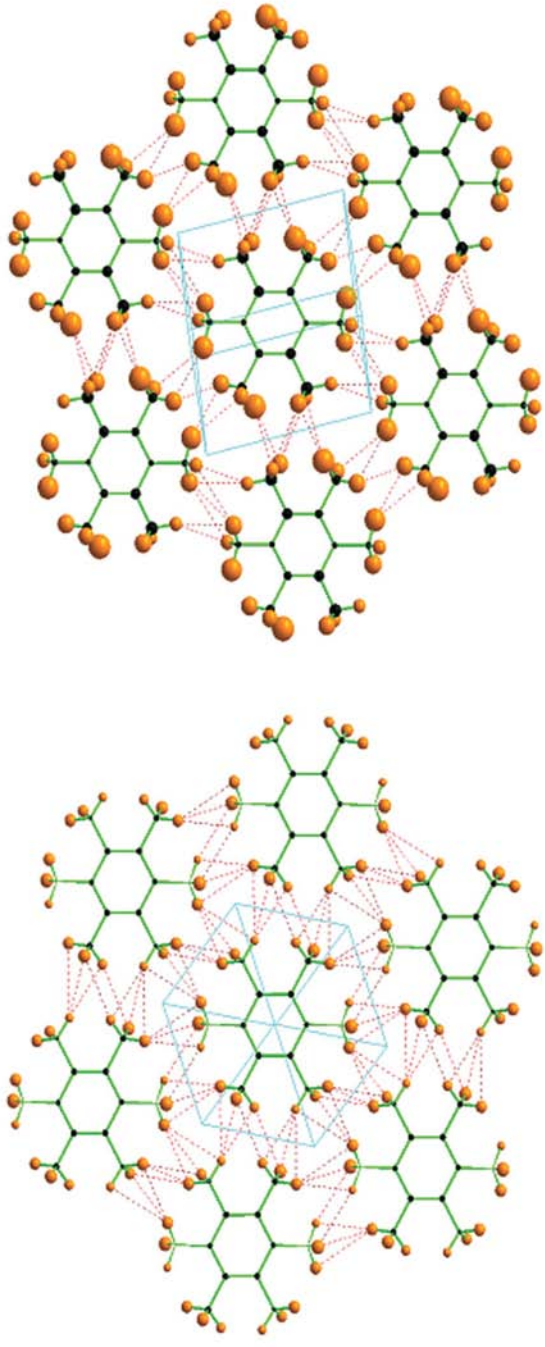

Figure 5
Shortest intermolecular interactions within the plane for phase II (upper) and phase III (lower).

the rings rotated by 10.6 (15)° about the normal to the molecular plane and away from the pseudo-rhombohedral high-symmetry sites. This molecular rotation acts to minimize the intermolecular Me repulsions, by displacing Me groups in adjacent layers relative to each other, resulting in an inter-Me distance 0.1 Å longer.

It is of interest to note in passing that the low-temperature crystal structure of d-benzene has a unit cell in which $\alpha = \beta = \gamma = 90°$, but which is longer along all axes: $a = 7.355$, $b = 9.371$, $c = 6.99$ Å (David *et al.*, 1992). However, the cell occupancy z is equal to 2, resulting in a molecular volume of 230.86 Å^3. This should be compared with the cell volume obtained here for HMB, equivalent to the molecular volume as $z = 1$, of 237.15 Å^3. The difference being 6.29 Å^3 or 1.05 Å^3 per methyl group, essentially the volume obtained for a cone-like methyl group, allowing for atomic radii at the proton positions. Hence, the low-temperature structures of both benzene and HMB are predominantly governed by space-filling considerations, with the increased bulk of HMB resulting in a different structure.

We will now move on to look at both the molecular geometry and the relative intermolecular stacking in III, drawing upon the structure of II for comparison.

3.1. Molecular geometry

In both phases II and III the aromatic rings were found to be planar, with the Me groups adopting an out-of-plane tilt angle, alternating above and below the plane, of 3.3 (4)° in phase III and 1.2 (1)° in phase II, Fig. 3. This agrees well with the value of 3.5 (3)° obtained in the previously reported single-crystal structure of phase II (Le Maguères *et al.*, 2001), with the relatively large discrepancy in phase II being due to the large isotropic displacement parameters limiting the precision with which this angle can be determined. The value of this tilt angle calculated for the lowest energy conformation for an isolated molecule is 4.8° (Gough *et al.*, 1985), indicating that the intramolecular repulsions between neighbouring Me groups on the same aromatic ring dominate the molecular geometry, confirmed here to be D_{3d} at low temperature, rather than C_{6h}. The Me groups also display a staggered conformation, with torsional angles such that neighbouring intramolecular groups interlock in a gear-type manner. This energy-minimization has been predicted in computational studies (Iroff, 1980; Gough *et al.*, 1985) and inferred from NMR studies on the solid (Takeda & Chihara, 1987; Takeda *et al.*, 1980).

Table 3
Intramolecular bond lengths (Å) in HMB.

T = 5 K		T = 140 K	
C—C (ring)	1.398 (10)	C—C (ring)	1.400 (4)
C—C (Me)	1.524 (6)	C—C (Me)	1.531 (3)
C—D (Me)	1.071 (5)	C—D (Me)	1.050 (6)

As may be expected for a covalently bonded molecular material, the intramolecular bond lengths show no significant temperature dependence, see Table 3. The aromatic C—C bonds were found to be 1.40 Å long and the ring-to-Me C—C bonds 1.53 Å in length, both values being typical of the respective bond orders. The C—D bond lengths, by contrast, do show a small expansion in the low-temperature structure, phase III, Δd_{C-D} = 0.021 (8) Å over that in phase II. This effect has previously been accounted for in a survey of reported neutron diffraction-derived C—H bond lengths (Steiner & Saenger, 1993), where it was noted that as a result of thermally induced vibrations in Me groups, the C—H bond length actually expands by an average of 0.03 Å in structures obtained at $T < 30$ K with respect to those measured at room temperature. The observed difference is also reflected in the pronounced increase in the isotropic atomic displacement factors for the deuterons of the Me groups in phase II over phase III, 6.9 (9) and 2.2 (2), respectively. Indeed, the role of ther-

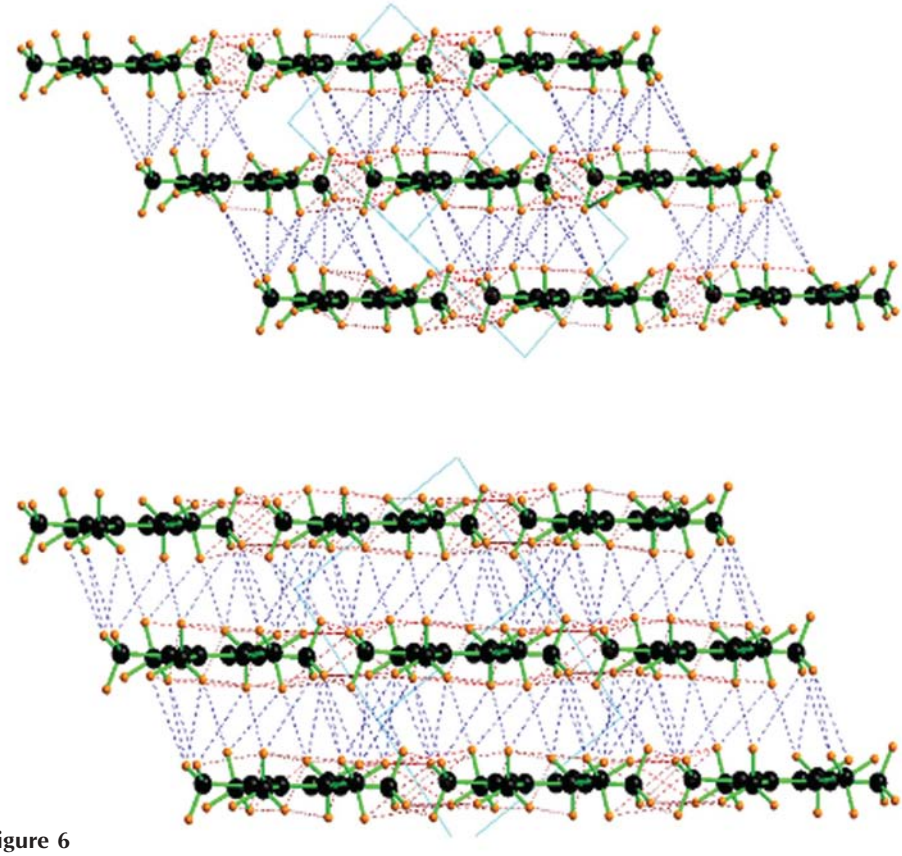

Figure 6
Shortest intermolecular interactions between the planes for phase II (upper) and phase III (lower), with in-plane interactions in red and inter-plane interactions in blue.

mally induced atomic displacements in the phase transition is clearly shown in Fig. 4. All of the atoms in HMB show a significant increase in the atomic displacement factors, $U_{iso}^{T=140K} = 2.8\ (6) \times U_{iso}^{T=5K}$, indicating that the phase transition is driven by the thermally induced disorder of the whole molecules. Indeed, the fact that the cell volume obtained herein at $T = 140$ K ($\sim 1.05 T_c^D$) displays a 1% contraction over that previously obtained at $\sim 1.05 T_c^H$ supports the conclusion that whole body molecular displacements play an important role in supporting the cell volume.

The Me groups can be described as being slightly distorted tetrahedra, with a mean $\angle$DCD(III) = 107.5 (8)° and $\angle$CCD(III) = 111.4 (6)° and for phase II, $\angle$DCD(II) = 108.5 (3)° and $\angle$CCD(II) = 110.0 (2)°, which are within the limits of the determination of Le Maguères *et al.* (2001), with $\angle$HCH(II) = 106.8 (17)° and $\angle$CCH(II) = 111.9 (6)°.

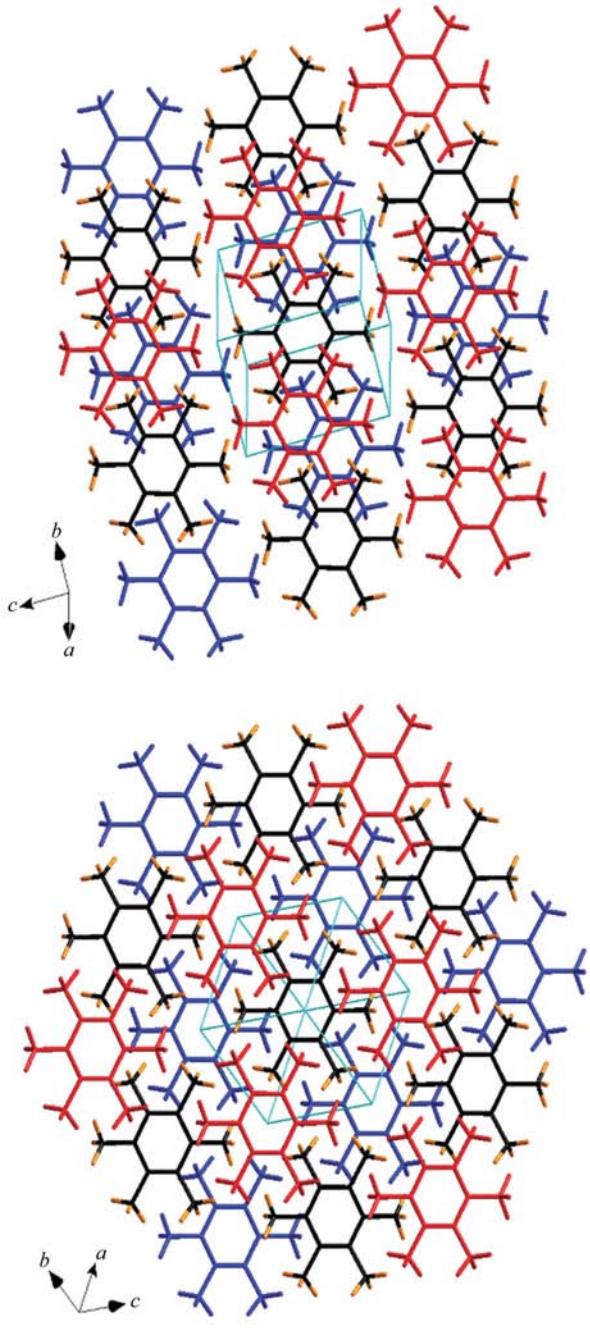

Figure 7
Comparison of phase II (upper) and phase III (lower) viewed along the normal to the molecular plane. Three layers are shown, with the lower layer in blue and the upper layer in red. The central layer has carbon atoms in black and deuterium atoms in orange.

3.2. Molecular packing

HMB molecules in both phases II and III lie within planes and so the intermolecular interactions can reasonably be divided into those between molecules within a single plane and those between molecules in neighbouring planes. In order to ensure a close packing of HMB molecules, a delicate balance between the intra-plane and the inter-plane repulsions is apparent. In phase II the mean shortest in-plane interactions are 2.79 (5) Å with the corresponding inter-planar distance of 2.73 (5) Å. By contrast, in phase III the respective lengths are 2.73 (6) and 2.70 (5) Å. Whilst these values are very similar for both phases, in phase III the molecules are more closely packed, with the intra- and inter-planar distances essentially equal. The largest difference in the intermolecular interactions between phase III and phase II is the average in-plane distance, with the inter-plane intercations remaining constant. The shortest in-plane interactions are shown in Fig. 5 and the inter-plane interactions are shown in Fig. 6.

As stated above, the structure of the low-temperature phase (III) can be considered to be pseudo-rhombohedral with a cubic close-packed (c.c.p.) arrangement, in which the molecular plane is approximately perpendicular to the (111) axis, Fig. 7, (111) in phase II. The c.c.p. arrangement of phase III is clearly seen in the ABC layers highlighted by colouring in Fig. 7. As such the first-order transition from phase III to phase II is best characterized as a shearing process between molecular layers. Along with this motion is an associated partial rotation of the Me groups. The layered stacking within HMB may be able to account for the largest differences in the fitted diffraction patterns, Fig. 1, which lie around the (111) peak at $2\theta \simeq 25.5°$ (III) and are probably due to stacking faults in the ABC system (ABABC, for example).

4. Conclusion

The low-temperature phase (III) of HMB has been shown to possess an increased packing density over the room-temperature phase (II), which in itself is also more dense than the plastic phase (I) found above $T = 383$ K (Spaght *et al.*, 1932). As such the first-order transition into phase III is driven by a relaxation of the crystal under decreasing thermal motions of individual molecules This aspect reiterates the isotopic dependence of the first order transition into phase III, whilst the confirmation of only a single molecule per unit cell brings the structural data into line with that obtained using spectroscopic methods.

The author would like to thank Mr P. Cross for technical assistance and Dr A. Hewat for discussions, both of ILL. In addition, the author is indebted to Dr A. Fitch of the ESRF for providing time on ID31 and greatly assisting with data analysis. This demonstrated that finite resolution does not obscure salient features in the neutron data. Of course, the author extends this acknowledgement to the technical services of the ESRF and management.

References

Accelrys Inc. (2003). *Materials Studio Modeling Environment*, Version 3.0.0.0. Accelrys Inc., San Diego.
Adams, J. M., Ivanov, A. S., Johnson, M. R. & Stride, J. A. (2004). *Physica B*, **350**, E351–E354.
Brockway, L. O. & Robertson, J. M. (1939). *J. Chem. Soc.* pp. 1324–1332.
Celotti, G., Bertinelli, F. & Stremmenos, C. (1975). *Acta Cryst.* A**31**, 582–585.
David, W. I. F., Ibberson, R. M., Jeffrey, G. A. & Ruble, J. R. (1992). *Physica B*, **180/181**, 597–600.
Dollase, W. A. (1986). *J. Appl. Cryst.* **19**, 267–272.
Fitch, A. N. (2004). *J. Res. Natl. Stand. Technol.* **109**, 133–142.
Fujiwara, T., Inaba, A., Atake, T. & Chihara, H. (1992). *J. Chem. Thermodyn.* **24**, 863–881.
Gough, K. M., Henry, B. R. & Wildman, T. A. (1985). *J. Mol. Struct. Theochem.* **124**, 71–85.
Hamilton, W. C., Edmonds, J. W., Tippe, A. & Rush, J. J. (1969). *Discuss. Faraday Soc.* **48**, 192–204.
Hewat, A. W. (1986). *Mater. Sci. Forum*, **9**, 69–79.
Howard, C. J. (1982). *J. Appl. Cryst.* **15**, 615–620.
Huffman, H. M., Parker, G. S. & Daniels, A. C. (1930). *J. Am. Chem. Soc.* **52**, 1547–1558.
Iroff, L. D. (1980). *J. Comput. Chem.* **1**, 76–80.
Larson, A. C. & Von Dreele, R. B. (2000). *General Structure Analysis System, GSAS*, Report 2000, LAUR 86-748. Los Alamos National Laboratory, New Mexico, USA.
Le Maguères, P., Lindeman, S. V. & Kochi, J. K. (2001). *Organometallics*, **20**, 115–125.
Lonsdale, K. (1929). *Trans. Faraday Soc.* **25**, 352–366.
Mizuno, M., Hamada, M., Hashimoto, M., Harada, M., Eda, K., Yamamura, K., Kamiyama, T. & Oikawa, K. (2004). *Powder Diffr.* **19**, 149–152.
Molecular Simulations Inc. (1995). *Cerius2 User's Guide.* Molecular Simulations Inc., San Diego, USA.
Neumann, M. A., Johnson, M. R., Radaelli, P. G., Trommsdorff, H. P. & Parker, S. F. (2001). *J. Chem. Phys.* **110**, 516–527.
Neumann, M. A., Press, W., Nöldeke, C., Asmussen, B., Prager, M. & Ibberson, R. M. (2003). *J. Chem. Phys.* **119**, 1586–1589.
Pawley, G. S. (1981). *J. Appl. Cryst.* **14**, 357–361.
Rietveld, H. M. (1969). *J. App. Cryst.* **2**, 65–71.
Ron, A. & Hyams, I. J. (1972). *Chem. Phys. Lett.* **17**, 557–560.
Spaght, M. E., Thomas, S. B. & Parks, G. S. (1932). *J. Phys. Chem.* **36**, 882–888.
Steiner, T. & Saenger, W. (1993). *Acta Cryst.* A**49**, 379–384.
Takeda, S. & Chihara, H. (1987). *Springer Proc. Phys.* **17**, 76–80.
Takeda, S., Soda, G. & Chihara, H. (1980). *Solid State Commun.* **36**, 445–448.
Takeshita, H., Suzuki, Y., Nibu, Y., Shimada, H. & Shimada, R. (1999). *Bull. Chem. Soc. Jpn*, **72**, 381–387.
Von Bougeard, D., Bleckmann, P. & Schrader, B. (1973). *Ber. Bunsenges. Phys. Chem.* **77**, 1059–1070.